bioRxiv preprint doi: https://doi.org/10.1101/2023.01.26.525745; this version posted January 26, 2023. The copyright holder for this preprint (which was not certified by peer review) is the author/funder, who has granted bioRxiv a license to display the preprint in perpetuity. It is made available under aCC-BY-NC-ND 4.0 International license.

The Glucocorticoid Receptor is Required for Efficient Aldosterone-Induced Transcription by the Mineralocorticoid Receptor

Thomas A. Johnson[1], Gregory Fettweis[1], Kaustubh Wagh[1,2], Brian Almeida-Prieto[3], Gordon L. Hager[1,*], Diego Alvarez de la Rosa[1,3,*]

[1]Laboratory of Receptor Biology and Gene Expression, National Cancer Institute, NIH, Building 41, 41 Library Drive, Bethesda, MD, USA; [2]Department of Physics, University of Maryland, College Park, 4296 Stadium Drive, College Park, MD, USA; [3]Departamento de Ciencias Médicas Básicas and Instituto de Tecnologías Biomédicas, Universidad de La Laguna, Campus de Ciencias de la Salud sn, 38200 San Cristóbal de La Laguna, Spain.

[*]Corresponding authors: G.L.H., hagerg@dce41.nci.nih.gov; D.A.d.l.R., dalrosa@ull.edu.es

Short title: GR potentiates aldosterone/MR action

Keywords: steroid receptors, heteromerization, chromatin binding, ChIP-seq, RNA-seq, single-molecule tracking.

Funding: Research was supported by grants from the Intramural Research Program of the National Institutes of Health, National Cancer Institute, Center for Cancer Research and by grant PID2019-105339RB-I00 (funded by MCIN/AEI/10.13039/501100011033 and "ERDF A way of making Europe", MICINN, Spain). D.A.d.l.R. was partially supported by PRX18/00498 (funded by *Programa Estatal de Promoción del Talento y su Empleabilidad en I+D+i, Subprograma Estatal de Movilidad, del Plan Estatal de I+D+I,* MICINN, Spain). B.A.-P. was supported by pre-doctoral fellowship BES-2017-082939 (funded by MCIN/AEI/ 10.13039/501100011033 and by "ESF Investing in your future").

Disclosure: The authors have nothing to disclose.

ABSTRACT

The glucocorticoid and mineralocorticoid receptors (GR and MR, respectively) have distinct, yet overlapping physiological and pathophysiological functions. There is strong indication that both receptors interact both functionally and physically, but the precise role of this interdependence is poorly understood. Here, we analyzed the impact of GR co-expression on MR genome-wide chromatin binding and transcriptional responses to aldosterone and glucocorticoids, both physiological ligands of this receptor. Our data show that GR co-expression alters MR genome-wide binding in a locus- and ligand-specific way. MR binding to consensus DNA sequences is affected by GR. Transcriptional responses of MR in the absence of GR are weak and show poor correlation with chromatin binding. In contrast, co-expression of GR potentiated MR-mediated transcription, particularly in response to aldosterone. Finally, single-molecule tracking of MR suggests that the presence of GR contributes to productive binding to chromatin. Together, our data indicate that co-expression of GR potentiates aldosterone-mediated MR transcriptional activity, even in the absence of glucocorticoids.

bioRxiv preprint doi: https://doi.org/10.1101/2023.01.26.525745; this version posted January 26, 2023. The copyright holder for this preprint (which was not certified by peer review) is the author/funder, who has granted bioRxiv a license to display the preprint in perpetuity. It is made available under aCC-BY-NC-ND 4.0 International license.

INTRODUCTION

Adrenal glands coordinate physiological responses to cope with stress, acute injury or prolonged deprivation of water and food. Two important categories of adrenal hormones mediate key specific homeostatic responses: glucocorticoids (cortisol and corticosterone) and mineralocorticoids (aldosterone). However, these hormones show significant promiscuity. An excess of glucocorticoid signaling produces mineralocorticoid-like effects, particularly hypertension (1). Conversely, an excess of mineralocorticoids can mimic glucocorticoid effects, such as glucose homeostasis dysregulation and development of metabolic syndrome (2). The molecular basis for this cross-talk is at least partially explained by the close evolutionary relation between the mineralocorticoid receptor (MR) and the glucocorticoid receptor (GR), which confer on them poor ligand specificity and overlapping modes of action (3,4). Both mineralocorticoid and glucocorticoid hormones potently activate MR (5). Since glucocorticoids circulate at concentrations several orders of magnitude higher than aldosterone, certain cells co-express MR with 11-β-hydroxysteroid dehydrogenase type 2 (11-β-HSD2), an enzyme that metabolizes glucocorticoids into their biologically-inactive 11-keto metabolites, creating a low-glucocorticoid milieu (6). In contrast to MR, GR is partially selective, with potent activation by glucocorticoids and weak activation by mineralocorticoids (7). GR expression is essentially ubiquitous, while MR expression is more restricted and generally at lower abundance, except in the hippocampus and aldosterone-target epithelia such as the renal collecting duct and distal colon, where MR and GR abundance is similar (8). This, together with co-expression or not of 11-β-HSD2, generates at least three scenarios for corticosteroid hormone receptor function: GR-mediated responses to glucocorticoids; GR/MR-mediated responses to glucocorticoids; MR-mediated responses to aldosterone in the presence of presumably inactive GR.

Both MR and GR share a highly conserved DNA-binding domain (DBD), which implies that they recognize with high affinity the same DNA consensus sequence, known as “hormone response element” (HRE) (9), and likely regulate a partially overlapping set of genes. The largest differences in the amino acid sequences of MR and GR proteins occur in the N-terminal domain (NTD) with *Mus musculus* MR containing over 100 more amino acids than *M. musculus* GR and only 29% similarity (Suppl. Fig. 1A). By contrast, the DBD and the ligand-binding domain (LBD) of MR and GR have 90% and 69% similarity, respectively. The NTD of MR has been shown to be important for gene regulation (10,11). The AF1 activation regions of the MR NTD appear to be separated into two distinct amino acid sequences, AF1a and AF1b, similar to the androgen or progesterone receptors but unlike GR, which has one central AF1 domain in its NTD (11-13). In addition, MR is reported to have a region with intrinsic inhibitory function placed between AF1a and AF1b (13). The divergent structure of MR and GR NTDs may account at least in part for differential, tissue-specific transcriptional responses (14,15).

To further complicate the picture, it has been conclusively demonstrated that MR and GR can physically interact, forming heteromers (16-22). Examination of the functional properties of MR/GR interaction has produced conflicting experimental results. Gene-reporter assays or studying the expression of specific genes indicate that GR may enhance MR transcriptional activity in certain cell lines (23,24), although it appears to be inhibitory or non-influential in others (16-18,25). A recent study performed in keratinocytes demonstrated that MR co-expression alters GR genomic binding and modulates the global transcriptional response to the synthetic glucocorticoid dexamethasone (26). MR expression was initially thought to be restricted to aldosterone-target epithelia. However, it is now accepted to be widely present in different organs and systems, although with characteristically low

bioRxiv preprint doi: https://doi.org/10.1101/2023.01.26.525745; this version posted January 26, 2023. The copyright holder for this preprint (which was not certified by peer review) is the author/funder, who has granted bioRxiv a license to display the preprint in perpetuity. It is made available under aCC-BY-NC-ND 4.0 International license.

levels of protein compared to GR. GR expression is ubiquitous and generally higher than MR (8), implying that MR will typically function in the presence of significant levels of GR. The functional effects of this co-expression are unclear. Data obtained *in vivo* suggests that both receptors may be needed for potent aldosterone biological effects (27,28). However, there are no studies to date directly analyzing the global influence of GR on MR-mediated transcriptional responses, whether driven by aldosterone or glucocorticoids.

Given the physical interaction between both factors, the molecular basis for their specific physiological roles, overlapping functions and pathological consequences of dysregulation can only be understood after clearly defining the consequences of co-expression in genome-wide studies. To this end, we took advantage of a well-characterized cellular system to study MR chromatin binding, gene regulation, and single-molecule dynamics in the presence or absence of GR. Our results indicate that GR profoundly affects MR genome-wide chromatin binding in a locus- and ligand-specific way and generally potentiates MR-mediated gene transcription, correlating with an apparent stabilization of MR productive chromatin binding.

RESULTS

To study genome-wide function of mammalian MR both in the presence and absence of the closely related GR, we stably introduced a GFP-tagged MR into a well-characterized GR knockout (GRKO) C127 mouse cell line and its parental line that has endogenous GR (29). The GFP-tag of the integrated MR is inserted after residue 147 of the N-terminus of the receptor, which has been shown to optimize its hormone response over an N-terminal GFP tag and it readily translocates to the nucleus with hormone (Suppl. Fig 1B-C; (30)). We collected genome-wide data sets for RNA expression and chromatin immunoprecipitation (ChIP) from the two MR cell lines before and after hormone treatments with 10nM aldosterone (Aldo) or with 100nM corticosterone (Cort), both saturating conditions for MR (7). As a control, we also used the same chromatin preparations in the MR parental cells to ChIP endogenous GR with Aldo or Cort. We also compare the MR hormone-mediated response to previously reported genome-wide wild type and mutant GR datasets from the same cell lines (29,31).

Co-expression of GR alters MR genome-wide binding in locus-specific and ligand-specific ways

We performed ChIP-Seq for MR in the GRKO cells and the parental cells to determine how the presence of GR may affect MR binding across the genome. We treated cells with vehicle, Aldo or Cort for 1 hour prior to sample collection to detect differences in MR chromatin binding with Aldo (MR specific) or with Cort, which activates both MR and GR (5,32,33). GRKO cells treated with Aldo have slightly stronger MR chromatin binding than with Cort, as seen by normalized ChIP-seq signal intensity (Fig. 1A, aggregate plots). A union list of 2403 called MR peaks in the GRKO cells distributes into three clusters: 164 Cort-specific peaks (cluster 1), 782 Aldo-specific peaks (cluster 2), and 1457 peaks that occur with either treatment (cluster 3). MR binding in the parental cells with endogenous GR stands in contrast to its binding in the GRKO cells, as Cort induces the strongest MR binding instead of Aldo (Fig. 1B, aggregate plots). A Union list of 1718 MR peaks in the parental cells distributes into two large clusters: 1213 Cort-specific peaks (cluster 4), 501 Aldo/Cort-shared peaks (cluster 5), and a small group of only four weak Aldo-specific peaks (not shown).

A comparison of genome-wide MR binding between the two cell lines indicates how much GR influences MR chromatin binding and this influence is likely related to MR-GR receptor interactions. A

bioRxiv preprint doi: https://doi.org/10.1101/2023.01.26.525745; this version posted January 26, 2023. The copyright holder for this preprint (which was not certified by peer review) is the author/funder, who has granted bioRxiv a license to display the preprint in perpetuity. It is made available under aCC-BY-NC-ND 4.0 International license.

union list of MR binding peaks across the 2 cell lines with either ligand has a total of 2983 unique peaks in 3 clusters (Fig. 1C, clusters 6-8; Suppl. Table 1). The 2403 MR peaks in the GRKO cells distribute into clusters 7 and 8 while the 1718 MR peaks in the parental cells distribute into clusters 6 and 8. The Cort-treated parental cells have 580 MR peaks (cluster 6) that do not occur in the GRKO cells with either ligand, suggesting Cort-liganded GR is required to enable MR binding at these sites. This requirement for Cort-liganded GR does not necessarily signify direct interaction or interdependence of the two nuclear receptors. GR binding could simply be causing chromatin accessibility changes at these sites which could then enable MR binding; however, binding site clusters 7 and 8 provide more compelling evidence for receptor interaction. Cluster 7 has 1265 peaks specific to the GRKO cell line (stronger peaks with Aldo treatment) indicating that in the parental cells Cort- or Aldo-liganded GR inhibits MR binding at these sites. The cluster 7 MR binding in the parental cells is even weaker with Aldo treatment, again anticorrelated with MR binding in the GRKO cells. The cluster 7 endogenous GR ChIP-Seq signal in the parental cells also has very low binding with Cort treatment and virtually no binding with Aldo, suggesting that Aldo-liganded GR cannot efficiently bind these sites. It is, thus, unlikely that GR is simply out-competing MR for these sites (34). The 1138 MR binding sites shared between the two cell lines (cluster 8) exhibit the strongest signal intensity; however, the sites show the weakest peak intensities when both receptors are present and liganded by Aldo. This observation suggests GR at 10nM Aldo treatment not only binds chromatin poorly, but also inhibits MR binding. The lower binding of Aldo-liganded GR (versus Cort-liganded GR) is directly shown by ChIP-Seq of the parental cells with a GR antibody (Fig. 1D).

These data suggest that liganded GR has a dominant effect on the binding of MR, both potentiating at some sites inaccessible to MR by itself (cluster 6) and reducing its binding at sites it can bind when acting in the absence of GR (clusters 7 and 8). These effects on MR binding at the clusters 7 and 8 could be due to GR not completely translocating to the nucleus with Aldo or that it reducing the chromatin accessibility of the binding site or, more likely, that mixed receptor heteromers have different binding efficacies. Very few GR binding events have been shown to reduce chromatin accessibility at the site of direct receptor binding (35). It appears that the type of ligand bound to the interacting receptors, Aldo or Cort, also affects both receptors' binding efficiencies, with Aldo reducing the binding efficiency of both MR and GR when the receptors occupy the nucleus together.

Motif analyses show that MR binding favors consensus NR3C1-4/AP1 motifs and is affected by GR

We performed separate motif analyses on clusters 6-8 from the 2983 MR binding sites that occur across the two cell lines. We used various known motifs in the Homer database (36) that reflect the 13mer NR3C1-4 steroid receptor consensus sequence GnACAnnnTGTnC as a proxy for an MR binding motif (Suppl. Table 2). The three Homer MR motifs range in the stringency to the above consensus sequence primarily at the position 1 "G", position 5 "A" or position 13 "C" while positions 3-4 and 9-11 are well conserved (Suppl. Fig. 2).

The 580 cluster 6 MR peaks that only occur in the parental cells with Cort treatment had some form of MR-like binding motif between 37-62% of sites. The prevalence of the consensus steroid hormone receptor motif likely enabled both GR and, subsequently, MR binding (34). The AP1-like nTGAnTCAn motif (Suppl. Table 2; Suppl. Fig. 2) occurred between 2-4% of sites while THRb, Runx1, ZNF domain and ETS motifs were also detected. The 1265 cluster 7 GRKO-specific MR peaks were less enriched for MR-like consensus motifs (11-26% of sites) while AP1-like motifs occurred more often at 8-

bioRxiv preprint doi: https://doi.org/10.1101/2023.01.26.525745; this version posted January 26, 2023. The copyright holder for this preprint (which was not certified by peer review) is the author/funder, who has granted bioRxiv a license to display the preprint in perpetuity. It is made available under aCC-BY-NC-ND 4.0 International license.

15% of sites (Suppl. Table 2). The 1138 MR peaks of cluster 8 that are shared across the two cell lines were as enriched as cluster 6 for MR-like binding motifs (36-62% of sites) and similarly or slightly less enriched as cluster 7 for AP1-like motifs (5-10% of sites).

The motif analyses align with the MR ChIP-seq data in that the GR-dependent cluster 6 MR peaks are more enriched than cluster 7 peaks for NR3C1-4 motifs. Our previous studies have shown GR to be capable of binding to inaccessible, nucleosomal sites prior to hormone with GRE consensus motifs (31,37) whereas GRKO-specific sites (cluster 7) may more often have factors like AP1 bound prior to hormone that enable MR binding (38). This is reflected in previously published chromatin accessibility data of GRKO cells that show higher ATAC signal in cluster 7 prior to hormone than in cluster 6 (Fig. 1C; (29)). Cluster 8 MR sites exhibit the highest receptor binding intensity and have relatively higher enrichment of NR3C1-4 motifs than cluster 7 and higher AP1 consensus motifs than cluster 6. Like cluster 7, cluster 8 also exhibits higher pre-hormone accessibility than cluster 6 (Fig. 1C).

MR exhibits weak transcriptional activity without GR

To explore how receptor binding is related to changes in gene expression, we performed genome-wide total RNA sequencing (RNA-Seq) before and after hormone treatments in the GRKO and parental cell lines. We compared the differential expression (DE) analysis of vehicle versus 2 hours of exposure to either hormone from each cell line. We chose a false discovery rate (FDR) cutoff of 0.01 as determined by DESeq2 (via Homer) (39) to determine which genes show a change in exon RNA levels after treatment using two to three biological replicates per condition.

The parental cells with endogenous GR treated with Cort exhibit the strongest hormone response in both the number of up- or down-regulated genes and quantitative changes in RNA levels after treatment (Suppl. Table 3). We categorized protein-coding genes that met our FDR cutoff and exhibited a hormone-dependent change in RNA levels of plus or minus Log2 0.5 or greater. The parental cells treated with Cort had 210 hormone-responsive genes compared to 53 genes when treated with Aldo, 52 of which are common to both hormone treatments (Fig. 2A). The GRKO cells exhibit a much-reduced response to both Cort and Aldo with 12 and 17 genes changed, respectively, 11 of which are common to both treatments and also overlap with the common responsive genes in the parental cells. Even among 30 genes shared between the two cell lines that meet the FDR criteria regardless of fold change, the hormone response in the GRKO cells is attenuated compared to the cells with GR (Fig. 2B). Among these 30 genes, the hormone dependent fold change in the GR expressing cell line is lower with Aldo treatment compared to Cort; however, in the GRKO cells the level of hormone response is similarly weak for either hormone compared to the gene responses in the parental cells. This indicates MR by itself is a poor transcriptional regulator with either Cort or Aldo. The higher gene response of the parental cells with Cort treatment can be primarily attributed to GR, its natural receptor. The number of Cort-responsive genes is similar to that obtained in these cells when treated with dexamethasone (31). However, the gene response of the parental cells is also greater for Aldo treatment suggesting that MR regulates genes better with its natural ligand in concert with Aldo-liganded GR. RNA-seq data from Aldo-treated parental cells without MR show only 4 genes that meet the FDR and FC cutoffs, none of which overlap with hormone-responsive genes in the MR expressing cell lines. (Fig. 2A; Suppl. Table 3). This shows that GR by itself cannot induce a significant transcriptional response when liganded to Aldo, only in conjunction with MR.

Intergenic eRNAs correlate with gene transcription

bioRxiv preprint doi: https://doi.org/10.1101/2023.01.26.525745; this version posted January 26, 2023. The copyright holder for this preprint (which was not certified by peer review) is the author/funder, who has granted bioRxiv a license to display the preprint in perpetuity. It is made available under aCC-BY-NC-ND 4.0 International license.

The RNA-Seq data are not in agreement with the MR and GR ChIP-Seq results discussed above if we consider overall ChIP signal (binding intensity and number of peaks) to correlate with gene response (40). Among the four experimental conditions (two cell lines and two hormones), the parental line treated with Aldo generates the fewest MR and GR peaks but exhibited the second strongest transcriptional response. The GRKO cell line generates a comparatively weak transcriptional response to both Aldo and Cort despite producing more ChIP peaks than the respective treatments in the GR-containing parental line. Within each cell line, the ChIP and the RNA results do correlate as Aldo induces slightly more genes and more ChIP peaks in the GRKO cells while Cort does the same in the parental line.

We used Homer to annotate the MR peaks in the 3 clusters of Fig. 1C to the closest gene *in cis* and detected if these closest genes are among the 211 MR-responsive genes of the parental cells. Among the 1138 GRKO/Parental shared peaks of cluster 8, 79 were closest to hormone responsive genes, while 28 and 32 peaks were closest to hormone responsive genes in Clusters 6 and 7, respectively (Suppl. Table 1). These results are in line with those obtained by Ueda et al., which identified 25 out of 1414 ChIP-seq peaks placed proximal to aldosterone-regulated genes, as determined by microarray analysis, including common MR/GR targets such as SGK1, GILZ or Tns1 (41). Hormone responsive genes were sometimes detected near peaks from more than one cluster (ex. Tns1, Glul) or even all three clusters (ex. Ampd3, Tgm2). Of the 11 common MR responsive genes in GRKO cells, 10 are linked to annotated peaks in clusters 1, 2 or 3. The remaining gene, CTGF, a known MR/Aldo target gene in the heart (42), has a nearby distal peak in cluster 3, but with a non-hormone responsive gene occurring closer to it detected by the Homer peak annotation. It is likely that MR binding at several loci near a hormone responsive gene contributes to its transcriptional response and these loci may occur in more than one of the clusters in Fig. 1B. However, the strongest MR binding sites (cluster 8), as measured by ChIP signal intensity, are associated in *cis* to the most hormone responsive genes.

Active enhancers produce short bidirectional RNAs, known as enhancer RNAs (eRNAs), at sites of transcription factor binding and actively transcribing genes (43,44). We used the total RNA-Seq data to look for eRNAs at intergenic MR ChIP peaks as an indication of such activity. We left out MR peaks annotated to intron, UTR, exon and promoter sites to avoid RNA signal made by transcription near or within gene bodies. Of the 2983 MR peaks that make up clusters 6-8, 1576 are classified as intergenic according to Homer. We plotted the intergenic eRNA signal at these peaks sorted as a subset of each cluster in Fig. 1C and by ChIP signal intensity (Fig. 3). The eRNA heatmaps show little hormone-dependent change in signal at intergenic peaks in the GRKO cells; while increases in signal can be observed in the parental cells, more so with Cort than Aldo. In the parental cells, the increase in eRNA levels correlate with MR ChIP signal intensity at all three clusters, with Cluster 8.1 showing more change in overall eRNA signal than either cluster 6.1 or cluster 7.1. Thus, eRNA signal correlates with MR ChIP binding signal in the Parental cells with GR present, but not in the GRKO cells. The overall eRNA signal also correlates with the overall transcriptional response at the gene level.

The MR NTD contributes to transcriptional activity

The RNA data demonstrate that MR binding alone (ChIP signal intensity) in the absence of GR is not sufficient to induce a robust transcriptional response at the gene level or even of eRNAs at sites of MR binding. This could be due to a few possibilities. (1) MR requires a cofactor that may be present in cell types that naturally express MR but is missing our mouse cell lines. The extent of the MR gene response to Aldo in the parental cells argues against this being a wide-ranging limitation to MR activity.

bioRxiv preprint doi: https://doi.org/10.1101/2023.01.26.525745; this version posted January 26, 2023. The copyright holder for this preprint (which was not certified by peer review) is the author/funder, who has granted bioRxiv a license to display the preprint in perpetuity. It is made available under aCC-BY-NC-ND 4.0 International license.

(2) MR requires the interaction of GR and works better in concert with it to produce a transcriptional response. The greater hormone response of the parental cells that express endogenous GR agrees with this inference. (3) The unique structure of the NTD of MR may convey an inhibitory effect on steroid responsive genes similar to that shown by Litwack and colleagues on the MR-responsive Na/K ATPase β1 gene (25) or through its recruitment of particular co-repressors as shown by Lombes and colleagues (13).

To further explore how the NTD of MR affects its genome-wide hormone response, we performed RNA-Seq using an NTD-truncation mutant (MR-580C) in both the GRKO and Parental cell lines (Fig. 4A). We categorized protein-coding genes that met our FDR cutoff (0.01) and exhibited a hormone-dependent change in RNA levels of plus or minus Log2 0.5 or greater FC. Like the full-length version of MR (MRwt), the MR-580C mutant exhibited a weak gene response in the GRKO cells with 11 and 20 MR-responsive genes to Cort and Aldo treatment, respectively (Fig. 4B; Suppl. Table 3). The presence of endogenous GR in the Parental cells appears to potentiate the transcriptional effects of the MR-580C. The Cort-treated Parental cells have 314 responsive genes that meet the FDR and FC cutoffs while the Aldo-treated have 41 genes that meet the cutoffs. Again, the larger number of responsive genes with Cort versus Aldo can be attributed mainly to the presence of endogenous GR, but MR-580C activates/represses more genes with Aldo treatment in the presence of GR than in the GRKO cells (Fig. 4B; Suppl. Table 3). A comparison of 218 genes Cort-responsive genes meeting only the FDR cutoff and common to the MRwt cells and MR-580C cells show overall similar hormone responses (Fig. 4C). A similar comparison of 59 genes with Aldo treatment often shows reduced gene responses with MR-580C compared to MRwt (Fig. 4D). These data suggest that the NTD of MR is indeed functional in our model cell lines and contributing to the hormone-dependent transcriptional response, especially with Aldo treatment in the presence of GR. The MR-580C data also indicate that the NTD of MR does not have an overall inhibitory effect on hormone-dependent transcriptional activity as MRwt response is as high or higher than MR-580C.

Single molecule tracking of MR suggests GR contributes to productive binding

Given that our overall ChIP-seq results do not explain well the global changes in MR-mediated transcription induced by GR co-expression, we tested whether GR-induced changes in MR chromatin binding and transcriptional activity correlate with altered receptor dynamics in the nucleus. We performed single-molecule tracking (SMT) of transiently transfected Halo-tagged Histone H2B (serving as a probe for chromatin) and Halo-tagged MR in the GRKO and the Parental cells to determine the spatiotemporal dynamics of MR under these conditions. We fluorescently labeled the Halo tags with low concentrations of organic dye (see methods; (45)), and imaged cell nuclei using highly inclined laminated optical sheet (HILO) microscopy (46). We are most interested in the spatial mobility of molecules that remain bound on the order of tens of seconds as they were shown to be correlated with transcriptional outcomes (47). We imaged the cells only every 200 milliseconds (to minimize photobleaching), with 10 millisecond exposures (to minimize motion blur) (48). We would like to note that at this frame rate, freely diffusing molecules will rapidly exit the focal plane preventing their systematic study. The temporal projection of a representative SMT movie along with overlaid tracks are shown in Fig. 5A.

We first estimate the photobleaching rate from the H2B survival distribution as described previously (see Methods) (49). We then calculated the photobleaching-corrected survival probability distributions for MR activated with Aldo or Cort in both the Parental and GRKO cell lines. Under all

bioRxiv preprint doi: https://doi.org/10.1101/2023.01.26.525745; this version posted January 26, 2023. The copyright holder for this preprint (which was not certified by peer review) is the author/funder, who has granted bioRxiv a license to display the preprint in perpetuity. It is made available under aCC-BY-NC-ND 4.0 International license.

conditions, MR exhibits power-law distributed dwell times (Fig. 5B, C). We find that GR has no significant effect on the dwell times of MR when activated by Aldo (Fig. 5B). On the other hand, when activated with Cort, the presence of GR leads to a significant increase in the dwell time of MR (Fig. 5C), suggesting that Cort-activated GR stabilizes MR interactions with chromatin.

A previous SMT and fluorescence recovery after photobleaching (FRAP) study of MR showed that in the absence of GR, there is no difference in the dwell time distribution and bound fraction of Aldo- and Cort-liganded MR (50). Consistent with this study, we also find no significant difference between the dwell time distribution of MR irrespective of ligand in the absence of GR (Fig. 5B, C). We next asked whether Aldo-liganded MR exhibits distinct mobility patterns in the presence or absence of GR, which might contribute to differences in transcriptional output.

To measure the spatial mobility of MR, we used a systems-level classification algorithm called perturbation expectation maximization version 2 (pEMv2) (51) to classify MR trajectories into different mobility states, as described in Wagh et al. (52) (see Methods). On our imaging timescales, histone H2B as well as ten different transcriptional regulators have been shown to occupy mainly two distinct low-mobility states (52). The lowest mobility state (state 1) has a smaller exploration diameter of approximately 130-180 nm while the second low-mobility state has a slightly larger exploration diameter of approximately 250-350 nm (52). We have shown previously that both states represent chromatin binding states, with binding in state 1 requiring an intact DNA-binding domain as well as domains important for the recruitment of cofactors (52). For steroid receptors (SRs), hormone activation results in a substantial increase in the population fraction of state 1, suggesting that state 1 is correlated with the activation status of SRs.

Like other steroid hormone receptors, liganded MR in both the Parental and GRKO cells also exhibits two low mobility states with distinct exploration areas when treated with either Cort or Aldo (Fig. 5D, E). Aldo-liganded MR in GRKO cells also exhibits a small fraction of a slow diffusive state (state 3). As mentioned previously, our imaging interval of 200 ms does not allow for the systematic study of diffusing molecules, hence we restrict our analysis to the two low-mobility states. While we do not observe a significant difference in the dwell times of Aldo-treated MR in the Parental and GRKO cell lines (Fig. 5B), we find an ~2-fold increase in the population fraction of state 1 for Aldo-treated MR in the Parental cell line as compared to that in the GRKO cell line. We also measured the transition probabilities among state 1, 2, and all other states detected by pEMv2 (Suppl. Fig. 3) using a previously described method (52). Along with an increase in the population fraction of state 1, in the Parental cell line, Aldo-liganded MR shows an increase in the probability of remaining in state 1 or switching from state 2 to state 1 (Suppl. Fig. 3 A-B) as compared to that in the GRKO cells. On the other hand, while GR extended MR dwell times when treated with Cort, there was no significant difference between the population fractions of the different states of transition probabilities in the Parental and GRKO cell lines (Figs. 5 D, E and Suppl. Fig. 3C-D). Thus, while the ChIP-seq results are at odds with the RNA-seq results (Figs. 1 and 2), a dynamic analysis provides the missing link: an increase in MR binding in state 1 (the mobility state associated with active SRs) (Fig. 5D) along with increased transitions into this state (Suppl. Fig. 3A-B) could account for the different transcriptional outcomes.

bioRxiv preprint doi: https://doi.org/10.1101/2023.01.26.525745; this version posted January 26, 2023. The copyright holder for this preprint (which was not certified by peer review) is the author/funder, who has granted bioRxiv a license to display the preprint in perpetuity. It is made available under aCC-BY-NC-ND 4.0 International license.

DISCUSSION

In this study, we have demonstrated the global importance of GR to enhance aldosterone-driven transcriptional function of MR. Because both receptors respond to Cort, we cannot distinguish the contribution of MR/GR interactions with this treatment using RNA-seq alone. We have shown that when liganded to Aldo or Cort, MR by itself binds to hormone response elements but cannot efficiently elicit a transcriptional response. In contrast, when acting in the presence of GR, Aldo-liganded MR can increase transcription of genes and at intergenic enhancers that it cannot efficiently induce on its own. Further, GR by itself cannot elicit a significant gene response when liganded to Aldo, where the hormone acts much like an antagonist by binding receptor without imparting a functional response (53). Thus, in the presence of Aldo, both receptors appear to act together, enhancing MR-mediated gene response. This correlates with GR-dependent altered single molecule dynamics of MR, with Aldo-liganded MR showing a 2-fold increase in the population fraction of state 1 in the presence of GR (Fig. 5D).

The MR/GR coactivation of genes occurs despite lower overall levels of genomic binding by both receptors when present in the nucleus together compared to MR alone, specifically with Aldo treatment. Aldo-induced MR ChIP-seq peak intensities are reduced in all 3 clusters in the presence of GR (parental cells) versus its absence (GRKO cells), as shown in Fig. 1B. This suggests that genomic binding of MR as measured by ChIP in and of itself is not singular in prompting a full gene response. GR also has much reduced binding when liganded to Aldo suggesting that the two receptors are not competing for binding at the same response elements. When Cort is the ligand, the level of MR binding increases simultaneously with GR binding and is higher than binding with Aldo. This is consistent with the observation that, when activated with Cort, GR stabilizes MR-binding, significantly extending MR dwell time on chromatin (Fig. 5C). This may indicate that interaction of the two sister-receptors likely imposes its effects by the recruitment of co-regulators necessary for modulating transcription and not via higher levels of binding. Having a hetero-multimer of Aldo-liganded GR and MR may more effectively recruit co-factors than MR can accomplish by itself. Further studies on co-factor recruitment and transcriptional response are needed to answer this question.

Starting with the original studies by Trapp et al. (22) and Liu et al. (18), it has long been known that MR and GR are able to form heterocomplexes, although the functional impact of this interaction has been elusive (16-22). The functional effect of GR on MR action has been mainly studied in the context of glucocorticoid signaling, based on the common assumption that in the presence of 11-β -HSD2, local glucocorticoid levels are very low and thus GR would be inactive and not affect Aldo-mediated MR activity. Reporter gene transactivation assays using low levels of cortisol stimulation (up to 10 nM, thus favoring MR over GR binding) showed increased transcriptional responses when both receptors were present (22). However, this result seems to be dependent on promoter context, since opposite results were obtained with a reporter assay using a different promoter (18). Evidence for a direct MR/GR interaction was later expanded to a negative GRE (nGRE), with data suggesting that heteromerization of MR and GR directly mediates corticosteroid-induced trans-repression of the 5-HT1A receptor promoter (23). Further work performed with rainbow trout MR and GR receptors using gene reporter assays suggested that MR-GR interaction may be involved in cortisol responses, with a dominant-negative role of MR in the process (54). Interestingly, this study found that MR inhibitory role persists even in the presence of its antagonist eplerenone, suggesting that MR transcriptional activity is not important in the process. Other reports agree with this notion, where MR plays a dominant-negative role on GR-mediated glucocorticoid-regulated gene expression, further suggesting that the NTD of MR is

bioRxiv preprint doi: https://doi.org/10.1101/2023.01.26.525745; this version posted January 26, 2023. The copyright holder for this preprint (which was not certified by peer review) is the author/funder, who has granted bioRxiv a license to display the preprint in perpetuity. It is made available under aCC-BY-NC-ND 4.0 International license.

the domain involved in this effect through heterodimerization (55). The importance of this domain is confirmed by our data, as shown in Fig. 4. Misfud et al. tested the relevance of MR and GR interaction in a more physiological context, testing MR and GR binding to GREs of common glucocorticoid-target genes (Fkbp5, Per1 and Sgk1) in hippocampal neurons after exposure of rats to environmental stressors (56). Their results are consistent with gene-dependent binding of MR and GR to GREs as homo- and/or heterodimers. GR binding seemed to facilitate MR binding to GREs in Fkbp5 and Per1 genes under high-glucocorticoid conditions. Taken together, these studies generally indicate that MR and GR co-expression may impact glucocorticoid-mediated gene expression, but are limited by the lack of genome-wide binding or transcriptional analyses. More recently, Rivers et al investigated the global effect of MR on GR genomic binding in transfected neuroblastoma N2a cells using ChIP-nexus (21). Their results show that MR and GR bind to overlapping, highly similar sites (58% of them with GRE motifs). RT-qPCR experiments measuring expression of selected genes (*Syt2*, *Sgk1*, *Dusp4* and *Ddc*) showed that MR expression alone produced modest changes in expression upon 100 nM Cort stimulation, while GR co-expression induced more potent changes. This last experiment does not allow differentiating between MR-mediated and GR-mediated transcriptional changes. Interestingly, mutations in the DBD of MR did not prevent this effect, which led the authors to propose a tethering mechanism where GR mediates MR interaction with chromatin (21).

Few studies have directly investigated the impact of GR on Aldo-mediated MR transcriptional activity. Tsugita et al. examined this question with neuroblastoma and colon carcinoma cell lines expressing MR in the absence or presence of co-transfected GR and using reporter gene assays (24). This study demonstrated a lack of Aldo-induced luciferase activity unless GR is co-transfected. This MR rescuing effect is specific for GR, since other steroid receptors such as PR, or AR did not have any effect. Interestingly, deletion analysis of GR demonstrates that DNA binding and possibly receptor heterodimerization are critical in potentiating MR activity.

What is the molecular basis for the modulation of MR transcriptional activity by GR? Our data indicates that global, steady-state binding of MR to chromatin is not predictive of transcriptional activity. Interestingly, MR seems to be intrinsically more stable in its interaction with DNA than GR, as shown by hormone washout experiments (20,21), but this does not explain the changes in transcription seen upon GR co-expression. It may be argued that the proposed tethering mechanism, where GR mediates MR indirect binding to DNA may play a role in explaining our results (21). In this scenario, the MR ChIP peaks detected in our experiments in GRKO and parental cell lines would not be directly comparable, since the latter would correspond to a different mode of interaction that is more productive transcriptionally. However, the fact that GR binds DNA poorly when Aldo is the ligand but still has a prominent effect on potentiating MR activity rules out this possibility. Interestingly, our SMT data supports the idea of GR-induced differences in the kinetics of MR interaction with DNA. This is consistent with a previous report showing higher *in vitro* stability of MR/GR-DNA complexes when compared to MR alone (22). The situation may be more complicated, since MR and GR appear to interact with a specific GRE (a known binding site in the Per1 gene) in a cyclical way, possibly alternating homo- and heterocomplexes (57). Unfortunately, this study did not address MR dynamic interaction with chromatin in cells where GR is absent, precluding a more detailed analysis of the impact of GR on MR kinetics. On the other hand, MR and GR's cyclical interaction with chromatin also apply when Aldo is used as agonist (57), consistent with our findings at a genome-wide level. This further reinforces the

bioRxiv preprint doi: https://doi.org/10.1101/2023.01.26.525745; this version posted January 26, 2023. The copyright holder for this preprint (which was not certified by peer review) is the author/funder, who has granted bioRxiv a license to display the preprint in perpetuity. It is made available under aCC-BY-NC-ND 4.0 International license.

idea that GR participates in modulating MR-mediated transcriptional responses even when Aldo is the agonist.

Our data suggest that MR has likely evolved to work in concert with its more transcriptionally active sister receptor, GR, which is present in most tissues, including those where MR plays important cellular functions. By studying Aldo-activated MR function in the presence and absence of GR we mimic MR function in mammalian tissues where GR is present but, via Cort inactivation by 11-β-HSD2, can bind only, or mainly to Aldo. This is likely physiologically relevant. Ackermann et al. showed that while MR is constitutively nuclear in the Aldo-sensitive distal nephron, GR responds to fluctuations in Aldo circulating levels, at least in rats (58). Specifically, when Aldo levels are lowered by dietary NaCl loading, GR is localized to the cytosol, while MR remains nuclear. It is necessary to totally abrogate Aldo synthesis by adrenalectomy to achieve cytosolic localization for both MR and GR (58). Given the high circulating glucocorticoid levels during the peak of the circadian rhythm, it is possible that small amounts of glucocorticoids reach MR, which has high affinity for them. However, low doses of glucocorticoids would not activate GR and therefore the situation would result in relatively low MR activity. Only an increase in Aldo, which would be sensed by MR and also partially by GR would result in a more prominent MR-mediated response. This is consistent with a mechanism where GR plays an important role in the Aldo response, as originally proposed by Geering et al. (28) and indirectly corroborated by experiments using targeted knockout of the MR in the renal collecting duct (59) or overexpression of the GR in the renal collecting duct (60). In general, progressive recruitment of GR may contribute to the modulation of MR in the Aldo-sensitive distal nephron. This mechanism may have an impact in situations of altered glucocorticoid and mineralocorticoid signaling, including those induced under pathological situations or by pharmacological treatment of patients.

MATERIAL AND METHODS

Plasmids constructs and mutagenesis

A fully functional mouse MR fluorescent derivative with insertion of eGFP after amino acid 147 has been previously described (30). eGFP-MR was subcloned in plasmid Donor-Rosa26_Puro_CMV (29), with CMV promoter-driven expression, a puromycin resistance cassette and homology recombination arms specific for the mouse Gt(ROSA)26Sor locus. pX330 CRISPR/Cas9 plasmid, containing a guide RNA sequence to target the Gt(ROSA)26Sor locus, was a gift from Feng Zhang (Addgene plasmid #42230; (61)). Halo-tagged derivatives of MR were constructed using In-Fusion cloning. The entire NTD of MR was deleted using the Quickchange XL mutagenesis kit, generating construct MR-580C. Halo-tagged histone H2B has been previously described (62,63). All constructs and mutations were confirmed by DNA sequencing.

Cell culture and generation of cell lines by CRISPR/cas9

Cell lines were grown in Dulbecco's modified Eagle's medium (DMEM, Gibco) supplemented with 5 µg/ml tetracycline (Sigma-Aldrich #T7660), 10% fetal bovine serum (Gemini), sodium pyruvate, nonessential amino acids, and 2 mM glutamine. Cells were maintained in a humidifier at 37C and 5% CO2. Cells were plated for experiments in DMEM supplemented with 10% charcoal/dextran-treated serum for 24 hrs prior to hormone treatment. Cell lines used in this study derive from mouse mammary carcinoma cell line C127 (RRID: CVCL_6550) cells. Knockout of endogenously-expressed GR generating GRKO cells has been previously described (29). Transient transfections were performed using Jetprime

bioRxiv preprint doi: https://doi.org/10.1101/2023.01.26.525745; this version posted January 26, 2023. The copyright holder for this preprint (which was not certified by peer review) is the author/funder, who has granted bioRxiv a license to display the preprint in perpetuity. It is made available under aCC-BY-NC-ND 4.0 International license.

(Polyplus) according to the manufacturer´s instructions. eGFP-tagged MR was stably integrated in the genome using CRISPR/Cas9. To that end cells were co-transfected with pX330 CRISPR/Cas9 plasmid with a donor plasmid containing eGFP-MR driven by the CMV promoter. Donor plasmid insertion was selected by puromycin treatment followed by fluorescence-activated cell sorting (FACS). Expression of MR in sorted polyclonal cell declined with time and therefore we selected stable lines by one additional round of FACS, followed by single-cell cloning. GFP-MR expression in individual clones was confirmed by confocal microscopy and western blot using monoclonal antibody rMR1-18 1D5 (developed by Gomez-Sanchez et al. (64), and obtained from the Developmental Studies Hybridoma Bank, created by the NICHD, National Institutes of Health and maintained at The University of Iowa, Department of Biology) as previously described (17). MR agonists aldosterone and corticosterone were obtained from Sigma and dissolved in ethanol. Cells were plated for experiments in DMEM growth medium supplemented with 10% charcoal/dextran-treated serum for 48hrs prior to hormone treatment. Subsequently, cells were left untreated or treated with 10 nM aldosterone or 100 nM corticosterone for the indicated periods of time. Control cells were treated with ethanol at the same dilution used for treatments (1:1000).

ChIP-seq and analysis

Cells were treated with vehicle, 10 nM aldosterone or 100 nM corticosterone for 1h. Chromatin crosslinking, preparation and immunoprecipitation was performed essentially as described (31). Briefly, chromatin crosslinking was performed using 1% formaldehyde added to culture medium for 5 min. After glycine quenching and washing with PBS, cells were recovered and chromatin extracted and sonicated (Bioruptor, Diagenode) to an average DNA length of 500 bp. For immunoprecipitation of GFP-MR, 600 µgs of chromatin were incubated with 25 µg anti-GFP antibody (Abcam #ab290).

The ChIP-Seq data were aligned to the mouse reference mm10 genome using Bowtie 2 with command Bowtie2 –p 8 –x bowtie2_ref/genome_prefix –U read1.fastq –S result.sam. Subsequent downstream analysis was performed using HOMER (65). Peaks in each dataset were called using the findPeaks function with style factor for TFs and the no treatment condition used as a control. Peak filtering was done with the following parameters; FDR<0.001, >5 FC over control, >5 FC over local background, and ntagThreshold >5 Peak clusters were identified by the mergePeaks command and sorted by cell type and treatment. Pre-defined motif searches were performed with findMotifsGenome.pl using -m known5.motif -mscore. Gene annotation of peaks used annotatePeaks.pl mm10 -gene.

RNA Isolation, qPCR and RNA-seq analysis

Cells treated with vehicle, 10 nM aldosterone or 100 nM corticosterone for 2 h prior to RNA isolation. Total RNA was isolated using a commercially available kit (Macherey-Nagel NucleoSpin RNA isolation), which included an in-column DNase digestion step. Purified RNA was quantified using spectrophotometry and frozen in aliquots at -80ºC. One aliquot was used to synthesize single-stranded cDNA starting from 1 µg of total RNA using a commercially available kit (iScript cDNA Synthesis Kit, Biorad).

RNA-seq included two to three biological replicates of each condition and used Illumina Novaseq with 150 bp stranded reads. RTA 2.4.11 was used for Base calling and Bcl2fastq 2.20 was used for demultiplexing allowing 1 mismatch. Cutadapt 1.18 was used for adapter removal and quality control. RNA-seq alignment to mouse mm10 genome was performed by STAR 2.70 using the default parameters with the following modifications: '--genomeDir mm10-125 --outSAMunmapped Within --outFilterType BySJout --outFilterMultimapNmax 20 --outFilterMismatchNmax 999 --outFilterMismatchNoverLmax 0.04 --alignIntronMin 20 --alignIntronMax 1000000 --alignMatesGapMax 1000000 --alignSJoverhangMin 8 --limitSjdbInsertNsj 2500000 --alignSJDBoverhangMin 1 --sjdbScore 1 --sjdbFileChrStartEnd mm10-

bioRxiv preprint doi: https://doi.org/10.1101/2023.01.26.525745; this version posted January 26, 2023. The copyright holder for this preprint (which was not certified by peer review) is the author/funder, who has granted bioRxiv a license to display the preprint in perpetuity. It is made available under aCC-BY-NC-ND 4.0 International license.

125/sjdbList.out.tab --sjdbGTFfile UCSC_mm10_genes.gtf --peOverlapNbasesMin 10 --alignEndsProtrude 10 ConcordantPair'. All RNA-seq biological replicates correlated well with each other. Subsequent downstream analysis was performed using HOMER pipeline. Briefly, we obtained raw count data using analyzeRepeats.pl, and then the raw counts were normalized by default size factors from DESeq2 routine 23 provided via getDiffExpression.pl. We obtained differential genes using DESeq2, which fits negative binomial generalized linear models for each gene and uses the Wald test for significance testing, based on the criteria of a false discovery rate (FDR) cutoff <0.01 and absolute log2 fold change (FC) > 0.5 between no treatment and 2Hrs hormone treatment. We included only protein coding genes that are annotated in the RefSeq database and included no non-coding RNA species.

Heatmap and aggregate plot generation

We used Deeptools to generate ChIP-seq and eRNA heatmaps and aggregate plots. We first generated read-normalized bigwig files from bam files using the bamCoverage -b [inputfile] -o [output.bigWig] -of bigwig --binSize 20 --effectiveGenomeSize 2652783500 --normalizeUsing RPGC. We generated matrix files using computeMatrix reference-point --referencePoint center -S [input.bigWig files] -R [peakfile.bed] -a 500 -o [matrix.gz] --sortRegions keep. We then generated heatmaps using plotHeatmap -m [matrix.gz] -o [HM.pdf] --sortRegions no --zMin --zMax --refPointLabel "0 " --yAxisLabel "Tag Density". The eRNA heatmaps used merged replicate RNA bam files from the RNA seq data to make bigwig files. Bam files were merged using samtools.

Single-molecule tracking

Transient transfections

GRKO or Parental cell lines were plated in complete medium in two-well LabTek II chamber slides. The next day, HaloTag MR or H2B constructs were transfected using jetOPTIMUS (Polyplus) following manufacturer's protocol. After incubation for 4 hours with the jetOPTIMUS reaction mix, the medium was replaced with DMEM medium supplemented with charcoal/dextran-stripped FBS. 24 hours later, cells were incubated for 20 min with 5 nM of the cell-permeant HaloTag ligand Janelia Fluor 646 (JF_{646}). After labeling, cells were washed three times for 15 min with phenol red-free DMEM media (Gibco) supplemented with charcoal/dextran-stripped FBS, followed by one last wash after 10 min, to remove unbound JF_{646}. Cells were then treated with 10 nM Aldo or 100 nM Cort for 30 min before imaging.

Microscopy

All single-molecule tracking was performed on a custom-built HILO microscopy described previously (48). The microscope is equipped with a 150 X, 1.45 NA objective, (Olympus Scientific Solutions, Waltham, MA, USA), an Evolve 512 EM-CCD camera (Photometrics, Tucson, AZ, USA), a 647 nm laser (Coherent OBIS 647LX) and an Okolab stage-top incubator with 5% CO_2 control. Images were collected every 200 ms with an exposure time of 10 ms and laser power of 0.85 mW at the objective. The pixel size for this microscope is 104 nm.

Tracking

Tracking was performed using TrackRecord v6, a custom MATLAB software freely available at Zenodo (https://doi.org/10.5281/zenodo.7558712) and has been described previously (49,63). We allowed a maximum jump of 4 pixels, shortest track of 6 frames, and a gap of 1 frame. For details, see Wagh et al. (52).

Survival probability distribution of dwell times and unbound fraction

bioRxiv preprint doi: https://doi.org/10.1101/2023.01.26.525745; this version posted January 26, 2023. The copyright holder for this preprint (which was not certified by peer review) is the author/funder, who has granted bioRxiv a license to display the preprint in perpetuity. It is made available under aCC-BY-NC-ND 4.0 International license.

The survival distribution was used to determine and implement photobleaching correction as described previously (49). Briefly, the jump histogram of H2B was used to determine two displacement thresholds, R_{min} (the jump distance of 99% of H2B molecules between consecutive frames) and R_{max} (the jump distance of 99% of H2B molecules over 6 frames). Track segments with a jump distance larger than R_{min} over consecutive frames or R_{max} over 6 frames were classified as unbound and used to calculate the unbound fraction as described previously (63).

We fit the H2B survival distribution to a triple exponential function and extracted the smallest exponential parameter as the photobleaching rate (49). The survival distribution of MR under various conditions were corrected for photobleaching using this photobleaching rate as described in (49). Photobleaching-corrected survival distributions for MR were fit to three models: a double exponential, triple exponential, and a power-law. Model fits were evaluated using a Bayesian Information Criterion (BIC) and Evidence criterion (49). Statistical comparisons of the survival distributions were done using a logrank test with alpha = 0.05. Two-tailed p-values are reported in Fig. 5.

Classification in mobility states using pEMv2

We ran pEMv2 (51) separately for each of the four conditions (Aldo/Cort in Parental/GRKO cell lines) with parameters as described in (52). Briefly, we split tracks into sub-tracks of 7 frames and allowed pEMv2 to explore 1 to 15 states, with 20 reinitializations, 200 perturbations, and up to 10,000 iterations. The convergence criterion for the change in the log-likelihood function was set to 10^{-7}. After running pEMv2, we obtain a discrete set of mobility states along with a posterior probability for each sub-track to belong to each state. Sub-tracks are assigned to the state for which they have the highest posterior probability. We only excluded sub-tracks for which the difference of two highest posterior probabilities was less than 0.2 to retain only those sub-tracks that had unambiguous state assignment. States that had a population fraction less than 5% were excluded from the MSD plots and population fraction calculations.

Transition probability analysis

Since states 1 and 2 represent most of the sub-tracks, all the other states detected by pEMv2 were grouped into a third “Other” state for this analysis. As described previously (52), transition probabilities among the three states were calculated for tracks that contain at least three sub-tracks. To ensure that the transition probabilities are different from those expected from a random ensemble of sub-tracks that have the same population fractions, we shuffled the sub-tracks among all the tracks to generate 1000 random ensembles. We then calculated the transition probabilities among the three states for each of these 1000 ensembles. The statistical significance for each transition probability is reported as the fraction of random ensembles that had a higher transition probability than the calculated transition probability.

ACKNOWLEDGEMENTS

The authors thank the National Cancer Institute Advanced Technology Program Sequencing Facility for sequencing services. This research used the NIH high-performance computing systems (Biowulf) for genomics analyses. The researchers also thank Tatiana Karpova and David Ball of the Optical Microscopy Core at the NCI, NIH for assistance with the single molecule tracking experiments.

bioRxiv preprint doi: https://doi.org/10.1101/2023.01.26.525745; this version posted January 26, 2023. The copyright holder for this preprint (which was not certified by peer review) is the author/funder, who has granted bioRxiv a license to display the preprint in perpetuity. It is made available under aCC-BY-NC-ND 4.0 International license.

FIGURE LEGENDS

Figure 1. Chip-Seq data. **A-B.** Comparison of MR binding after 1 Hr. treatment with vehicle, 100nM Cort or 10nM Aldo in two cell lines (GRKO with no GR or Parental with endogenous GR). Aggregate plots represent total ChIP-Seq tag density of all peaks normalized as reads per genomic content (1x normalization). Heatmaps represents ± 500bp around the center of the MR peak. ChIP-Seq intensity scale is noted lower right on a linear scale. Clusters of peaks are labeled on the left with the peak number in parentheses and are sorted from high to low signal for the condition with the highest overall signal. A small cluster of four Aldo-specific peaks in the parental cells are not shown on the heatmap. **C-D.** A union list of MR ChIP peaks from A-B was created (see methods) and clustered by cell line and hormone treatment. 2983 unique MR peaks are distributed into Parental-specific/Cort (cluster6), GRKO-specific/Aldo (cluster 7) or shared between to two cell types (cluster 8). Aggregate plots and heatmaps are displayed as described for A-B for both MR ChIP and endogenous GR ChIP (parental cells only). ATAC-seq data are from untreated GRKO cells with stably expressed GFP-GRwt (29). The ATAC data heatmap is sorted the same as ChIP data in C and intensity scale is noted lower right on a linear scale.

Figure 2. MR hormone response in the presence or absence of GR. **A.** Venn diagrams of hormone-regulated protein-coding genes (2 Hrs. treatment/vehicle) to 100nM Cort or 10nM Aldo. Total number of hormone responsive genes (FDR $\leq$ 0.01, Log2 FC $\geq$ +/- 0.5) denoted in parentheses for MR expressing GRKO cells, MR expressing Parental cells or Parental cells without MR. Circles connected with lines denote 11 common hormone-responsive genes to the two cell lines. **B.** Scatter plot of Log2 FC for 30 genes common (meet FDR 0.01 cutoff only) to the four denoted conditions. Box and whiskers plot of the same data display interquartile range (IQR) depicting the 25th, 50th and 75th percentile as box with the median as black bar. The whiskers mark the most induced and repressed genes.

Figure 3. eRNA Signal at intergenic MR Peaks. The left heatmap shows subsets of clusters 6-8 (Fig 1C) representing intergenic MR ChIP peaks. Aggregate plots represent total ChIP-Seq tag density of all peaks normalized as reads per genomic content (1x normalization). Heatmaps represents ± 1kb around the center of the MR peak. ChIP-Seq intensity scale is noted lower right on a linear scale. Clusters of peaks are labeled on the left with the peak number in parentheses and are sorted from high to low signal for the condition with the highest overall signal. The right heatmap shows total normalized RNA-seq signal from merged replicates in the same order and breadth as the MR-ChIP heatmaps. Aggregate plots represent total RNA-Seq tag density normalized as reads per genomic content (1x normalization). RNA-Seq intensity scale is noted lower left on a linear scale.

Figure 4. MR 580C hormone response. **A.** Gene diagram of the stably expressed the MR NTD mutant. **B.** Venn diagrams of hormone-regulated protein-coding genes (2 Hrs. treatment/vehicle) to 100nM Cort or 10nM Aldo. Total number of hormone responsive genes (FDR $\leq$ 0.01, Log2 FC $\geq$ +/- 0.5) denoted in parentheses for MR expressing GRKO cells or MR expressing Parental cells (with endogenous GR). Circles connected with lines denote common hormone-responsive genes to the two cell lines. **C.** Scatter plot of Log2 FC for 218 Cort-responsive genes in the Parental cells common (meet FDR 0.01 cutoff only) to MRwt (Fig.2A) and MR580C. Box and whiskers plot of the same data display interquartile range (IQR) depicting the 25th, 50th and 75th percentile as box with the median as black bar. The whiskers mark the most induced and repressed genes. **D.** Scatter and Box and Whiskers plots of Log2 FC for 39 Aldo-responsive genes in the Parental cells common to MRwt and MR580C, as described above.

bioRxiv preprint doi: https://doi.org/10.1101/2023.01.26.525745; this version posted January 26, 2023. The copyright holder for this preprint (which was not certified by peer review) is the author/funder, who has granted bioRxiv a license to display the preprint in perpetuity. It is made available under aCC-BY-NC-ND 4.0 International license.

Figure 5. Single molecule tracking of MR. **A.** Temporal projection of an MR single molecule tracking movie (left) overlaid with tracks (right). Scale bar 5 μm **B.** Photobleaching corrected survival probability distributions of MR dwell times upon activation by aldosterone (Aldo) in the Parental (red circles) and GRKO (green diamonds) cell lines. Dashed lines indicate power-law fit to the survival distributions. P-value denotes the result of a logrank test. **C.** Survival distribution of MR dwell times upon activation by corticosterone (Cort) in the Parental (gray circles) and GRKO (blue diamonds) cell lines. Dashed lines indicate power-law fit to the data. The reported p-value is from a logrank test. **D-E.** (left) Ensemble mean-squared displacement (MSD) for the multiple mobility states determined by pEMv2 for MR activated with Aldo (D) and Cort (E). States for the Parental cell line are represented by dashed lines and those for the GRKO cell line are represented by solid lines. Error bars denote the standard error of the mean. (right) Population fractions for the different mobility states for MR activated with Aldo (D) and Cort (E). $N_{cells}/N_{tracks}/N_{sub\text{-}tracks}$: 51/2283/4802 (GRKO MR-Aldo), 51/2407/4750 (GRKO MR-Cort), 57/2965/5962 (Parental MR-Aldo), 60/2450/5730 (Parental MR-Cort). Two biological replicates were collected for each condition.

Suppl. Fig. 1. A. Sequence comparison between *M. musculus* MR and GR NTD. **B**. Schematic representation of M. musculus MR indicating the eGFP insertion site and the structure of the Donor-Rosa26_Puro_CMV-eGFP-MR vector. **C**. Representative confocal images showing eGFP-MR expression in a stable cell line and nuclear translocation after 1h 10 nM aldosterone treatment.

Suppl. Fig. 2. Position weight matrix logos used by HOMER program and prevalence of the consensus steroid hormone receptor motif.

Suppl. Fig 3. Switching characteristics of MR. Transition probabilities for MR among the different mobility states for MR activated by aldosterone (Aldo) in GRKO **(A)** and Parental **(B)** cell lines and MR activated by corticosterone (Cort) in GRKO **(C)** and Parental **(D)** cell lines. Cyan swarm charts depict the results of transition probability calculations for 1000 randomized ensembles of sub-tracks with the same population fractions. The fraction of randomized trials with a transition probability higher than the corresponding calculated transition probability are presented above the bars.

REFERENCES

1. Hunter RW, Ivy JR, Bailey MA. Glucocorticoids and renal Na+ transport: implications for hypertension and salt sensitivity. *J Physiol*. 2014;592(8):1731-1744.
2. Fallo F, Veglio F, Bertello C, Sonino N, Della Mea P, Ermani M, Rabbia F, Federspil G, Mulatero P. Prevalence and characteristics of the metabolic syndrome in primary aldosteronism. *J Clin Endocrinol Metab*. 2006;91(2):454-459.
3. Baker ME. Steroid receptors and vertebrate evolution. *Mol Cell Endocrinol*. 2019;496:110526.
4. Bridgham JT, Carroll SM, Thornton JW. Evolution of hormone-receptor complexity by molecular exploitation. *Science*. 2006;312(5770):97-101.
5. Arriza JL, Weinberger C, Cerelli G, Glaser TM, Handelin BL, Housman DE, Evans RM. Cloning of human mineralocorticoid receptor complementary DNA: structural and functional kinship with the glucocorticoid receptor. *Science*. 1987;237(4812):268-275.
6. Chapman K, Holmes M, Seckl J. 11beta-hydroxysteroid dehydrogenases: intracellular gate-keepers of tissue glucocorticoid action. *Physiol Rev*. 2013;93(3):1139-1206.

bioRxiv preprint doi: https://doi.org/10.1101/2023.01.26.525745; this version posted January 26, 2023. The copyright holder for this preprint (which was not certified by peer review) is the author/funder, who has granted bioRxiv a license to display the preprint in perpetuity. It is made available under aCC-BY-NC-ND 4.0 International license.

7. Hellal-Levy C, Couette B, Fagart J, Souque A, Gomez-Sanchez C, Rafestin-Oblin M. Specific hydroxylations determine selective corticosteroid recognition by human glucocorticoid and mineralocorticoid receptors. *FEBS Lett*. 1999;464(1-2):9-13.
8. Farman N, Rafestin-Oblin ME. Multiple aspects of mineralocorticoid selectivity. *Am J Physiol Renal Physiol*. 2001;280(2):F181-192.
9. Hudson WH, Youn C, Ortlund EA. Crystal structure of the mineralocorticoid receptor DNA binding domain in complex with DNA. *PLoS One*. 2014;9(9):e107000.
10. Fischer K, Kelly SM, Watt K, Price NC, McEwan IJ. Conformation of the mineralocorticoid receptor N-terminal domain: evidence for induced and stable structure. *Mol Endocrinol*. 2010;24(10):1935-1948.
11. Fuse H, Kitagawa H, Kato S. Characterization of transactivational property and coactivator mediation of rat mineralocorticoid receptor activation function-1 (AF-1). *Mol Endocrinol*. 2000;14(6):889-899.
12. Lavery DN, McEwan IJ. Structure and function of steroid receptor AF1 transactivation domains: induction of active conformations. *Biochem J*. 2005;391(Pt 3):449-464.
13. Tallec LP, Kirsh O, Lecomte MC, Viengchareun S, Zennaro MC, Dejean A, Lombes M. Protein inhibitor of activated signal transducer and activator of transcription 1 interacts with the N-terminal domain of mineralocorticoid receptor and represses its transcriptional activity: implication of small ubiquitin-related modifier 1 modification. *Mol Endocrinol*. 2003;17(12):2529-2542.
14. Gomez-Sanchez E, Gomez-Sanchez CE. The multifaceted mineralocorticoid receptor. *Compr Physiol*. 2014;4(3):965-994.
15. Meijer OC, Buurstede JC, Viho EMG, Amaya JM, Koning A, van der Meulen M, van Weert L, Paul SN, Kroon J, Koorneef LL. Transcriptional glucocorticoid effects in the brain: Finding the relevant target genes. *J Neuroendocrinol*. 2022:e13213.
16. Bigas J, Sevilla LM, Carceller E, Boix J, Perez P. Epidermal glucocorticoid and mineralocorticoid receptors act cooperatively to regulate epidermal development and counteract skin inflammation. *Cell Death Dis*. 2018;9(6):588.
17. Jimenez-Canino R, Fernandes MX, Alvarez de la Rosa D. Phosphorylation of Mineralocorticoid Receptor Ligand Binding Domain Impairs Receptor Activation and Has a Dominant Negative Effect over Non-phosphorylated Receptors. *J Biol Chem*. 2016;291(36):19068-19078.
18. Liu W, Wang J, Sauter NK, Pearce D. Steroid receptor heterodimerization demonstrated in vitro and in vivo. *Proc Natl Acad Sci U S A*. 1995;92(26):12480-12484.
19. Nishi M, Tanaka M, Matsuda K, Sunaguchi M, Kawata M. Visualization of glucocorticoid receptor and mineralocorticoid receptor interactions in living cells with GFP-based fluorescence resonance energy transfer. *J Neurosci*. 2004;24(21):4918-4927.
20. Pooley JR, Rivers CA, Kilcooley MT, Paul SN, Cavga AD, Kershaw YM, Muratcioglu S, Gursoy A, Keskin O, Lightman SL. Beyond the heterodimer model for mineralocorticoid and glucocorticoid receptor interactions in nuclei and at DNA. *PLoS One*. 2020;15(1):e0227520.
21. Rivers CA, Rogers MF, Stubbs FE, Conway-Campbell BL, Lightman SL, Pooley JR. Glucocorticoid Receptor-Tethered Mineralocorticoid Receptors Increase Glucocorticoid-Induced Transcriptional Responses. *Endocrinology*. 2019;160(5):1044-1056.
22. Trapp T, Rupprecht R, Castren M, Reul JM, Holsboer F. Heterodimerization between mineralocorticoid and glucocorticoid receptor: a new principle of glucocorticoid action in the CNS. *Neuron*. 1994;13(6):1457-1462.
23. Ou XM, Storring JM, Kushwaha N, Albert PR. Heterodimerization of mineralocorticoid and glucocorticoid receptors at a novel negative response element of the 5-HT1A receptor gene. *J Biol Chem*. 2001;276(17):14299-14307.
24. Tsugita M, Iwasaki Y, Nishiyama M, Taguchi T, Shinahara M, Taniguchi Y, Kambayashi M, Nishiyama A, Gomez-Sanchez CE, Terada Y, Hashimoto K. Glucocorticoid receptor plays an indispensable role in mineralocorticoid receptor-dependent transcription in GR-deficient BE(2)C and T84 cells in vitro. *Mol Cell Endocrinol*. 2009;302(1):18-25.
25. Derfoul A, Robertson NM, Hall DJ, Litwack G. The N-terminal domain of the mineralocorticoid receptor modulates both mineralocorticoid receptor- and glucocorticoid receptor-mediated transactivation from Na/K ATPase beta1 target gene promoter. *Endocrine*. 2000;13(3):287-295.

bioRxiv preprint doi: https://doi.org/10.1101/2023.01.26.525745; this version posted January 26, 2023. The copyright holder for this preprint (which was not certified by peer review) is the author/funder, who has granted bioRxiv a license to display the preprint in perpetuity. It is made available under aCC-BY-NC-ND 4.0 International license.

26. Carceller-Zazo E, Sevilla LM, Pons-Alonso O, Chiner-Oms A, Amazit L, An Vu T, Vitellius G, Viengchareun S, Comas I, Jaszczyszyn Y, Abella M, Alegre-Marti A, Estebanez-Perpina E, Lombes M, Perez P. The mineralocorticoid receptor modulates timing and location of genomic binding by glucocorticoid receptor in response to synthetic glucocorticoids in keratinocytes. *FASEB J*. 2023;37(1):e22709.
27. Gaeggeler HP, Gonzalez-Rodriguez E, Jaeger NF, Loffing-Cueni D, Norregaard R, Loffing J, Horisberger JD, Rossier BC. Mineralocorticoid versus glucocorticoid receptor occupancy mediating aldosterone-stimulated sodium transport in a novel renal cell line. *J Am Soc Nephrol*. 2005;16(4):878-891.
28. Geering K, Claire M, Gaeggeler HP, Rossier BC. Receptor occupancy vs. induction of Na+-K+-ATPase and Na+ transport by aldosterone. *Am J Physiol*. 1985;248(1 Pt 1):C102-108.
29. Paakinaho V, Johnson TA, Presman DM, Hager GL. Glucocorticoid receptor quaternary structure drives chromatin occupancy and transcriptional outcome. *Genome Res*. 2019;29(8):1223-1234.
30. Aguilar-Sanchez C, Hernandez-Diaz I, Lorenzo-Diaz F, Navarro JF, Hughes TE, Giraldez T, Alvarez de la Rosa D. Identification of permissive insertion sites for generating functional fluorescent mineralocorticoid receptors. *Endocrinology*. 2012;153(7):3517-3525.
31. Johnson TA, Paakinaho V, Kim S, Hager GL, Presman DM. Genome-wide binding potential and regulatory activity of the glucocorticoid receptor's monomeric and dimeric forms. *Nat Commun*. 2021;12(1):1987.
32. Arriza JL, Simerly RB, Swanson LW, Evans RM. The neuronal mineralocorticoid receptor as a mediator of glucocorticoid response. *Neuron*. 1988;1(9):887-900.
33. Lombes M, Kenouch S, Souque A, Farman N, Rafestin-Oblin ME. The mineralocorticoid receptor discriminates aldosterone from glucocorticoids independently of the 11 beta-hydroxysteroid dehydrogenase. *Endocrinology*. 1994;135(3):834-840.
34. Voss TC, Schiltz RL, Sung MH, Yen PM, Stamatoyannopoulos JA, Biddie SC, Johnson TA, Miranda TB, John S, Hager GL. Dynamic exchange at regulatory elements during chromatin remodeling underlies assisted loading mechanism. *Cell*. 2011;146(4):544-554.
35. John S, Sabo PJ, Thurman RE, Sung MH, Biddie SC, Johnson TA, Hager GL, Stamatoyannopoulos JA. Chromatin accessibility pre-determines glucocorticoid receptor binding patterns. *Nat Genet*. 2011;43(3):264-268.
36. Benner C. http://homer.ucsd.edu/homer/motif/HomerMotifDB/homerResults.html.
37. Johnson TA, Chereji RV, Stavreva DA, Morris SA, Hager GL, Clark DJ. Conventional and pioneer modes of glucocorticoid receptor interaction with enhancer chromatin in vivo. *Nucleic Acids Res*. 2018;46(1):203-214.
38. Biddie SC, John S, Sabo PJ, Thurman RE, Johnson TA, Schiltz RL, Miranda TB, Sung MH, Trump S, Lightman SL, Vinson C, Stamatoyannopoulos JA, Hager GL. Transcription factor AP1 potentiates chromatin accessibility and glucocorticoid receptor binding. *Mol Cell*. 2011;43(1):145-155.
39. Love MI, Huber W, Anders S. Moderated estimation of fold change and dispersion for RNA-seq data with DESeq2. *Genome Biol*. 2014;15(12):550.
40. Carroll JS, Liu XS, Brodsky AS, Li W, Meyer CA, Szary AJ, Eeckhoute J, Shao W, Hestermann EV, Geistlinger TR, Fox EA, Silver PA, Brown M. Chromosome-wide mapping of estrogen receptor binding reveals long-range regulation requiring the forkhead protein FoxA1. *Cell*. 2005;122(1):33-43.
41. Ueda K, Fujiki K, Shirahige K, Gomez-Sanchez CE, Fujita T, Nangaku M, Nagase M. Genome-wide analysis of murine renal distal convoluted tubular cells for the target genes of mineralocorticoid receptor. *Biochem Biophys Res Commun*. 2014;445(1):132-137.
42. Messaoudi S, Gravez B, Tarjus A, Pelloux V, Ouvrard-Pascaud A, Delcayre C, Samuel J, Launay JM, Sierra-Ramos C, Alvarez de la Rosa D, Clement K, Farman N, Jaisser F. Aldosterone-specific activation of cardiomyocyte mineralocorticoid receptor in vivo. *Hypertension*. 2013;61(2):361-367.
43. Kim TK, Hemberg M, Gray JM, Costa AM, Bear DM, Wu J, Harmin DA, Laptewicz M, Barbara-Haley K, Kuersten S, Markenscoff-Papadimitriou E, Kuhl D, Bito H, Worley PF, Kreiman G, Greenberg ME. Widespread transcription at neuronal activity-regulated enhancers. *Nature*. 2010;465(7295):182-187.
44. Zhu C, Li L, Zhang Z, Bi M, Wang H, Su W, Hernandez K, Liu P, Chen J, Chen M, Huang TH, Chen L, Liu Z. A Non-canonical Role of YAP/TEAD Is Required for Activation of Estrogen-Regulated Enhancers in Breast Cancer. *Mol Cell*. 2019;75(4):791-806 e798.

bioRxiv preprint doi: https://doi.org/10.1101/2023.01.26.525745; this version posted January 26, 2023. The copyright holder for this preprint (which was not certified by peer review) is the author/funder, who has granted bioRxiv a license to display the preprint in perpetuity. It is made available under aCC-BY-NC-ND 4.0 International license.

45. Grimm JB, English BP, Chen J, Slaughter JP, Zhang Z, Revyakin A, Patel R, Macklin JJ, Normanno D, Singer RH, Lionnet T, Lavis LD. A general method to improve fluorophores for live-cell and single-molecule microscopy. *Nat Methods*. 2015;12(3):244-250, 243 p following 250.
46. Tokunaga M, Imamoto N, Sakata-Sogawa K. Highly inclined thin illumination enables clear single-molecule imaging in cells. *Nat Methods*. 2008;5(2):159-161.
47. Stavreva DA, Garcia DA, Fettweis G, Gudla PR, Zaki GF, Soni V, McGowan A, Williams G, Huynh A, Palangat M, Schiltz RL, Johnson TA, Presman DM, Ferguson ML, Pegoraro G, Upadhyaya A, Hager GL. Transcriptional Bursting and Co-bursting Regulation by Steroid Hormone Release Pattern and Transcription Factor Mobility. *Mol Cell*. 2019;75(6):1161-1177 e1111.
48. Paakinaho V, Presman DM, Ball DA, Johnson TA, Schiltz RL, Levitt P, Mazza D, Morisaki T, Karpova TS, Hager GL. Single-molecule analysis of steroid receptor and cofactor action in living cells. *Nat Commun*. 2017;8:15896.
49. Garcia DA, Fettweis G, Presman DM, Paakinaho V, Jarzynski C, Upadhyaya A, Hager GL. Power-law behavior of transcription factor dynamics at the single-molecule level implies a continuum affinity model. *Nucleic Acids Res*. 2021;49(12):6605-6620.
50. Groeneweg FL, van Royen ME, Fenz S, Keizer VI, Geverts B, Prins J, de Kloet ER, Houtsmuller AB, Schmidt TS, Schaaf MJ. Quantitation of glucocorticoid receptor DNA-binding dynamics by single-molecule microscopy and FRAP. *PLoS One*. 2014;9(3):e90532.
51. Koo PK, Mochrie SG. Systems-level approach to uncovering diffusive states and their transitions from single-particle trajectories. *Phys Rev E*. 2016;94(5-1):052412.
52. Wagh K, Stavreva DA, Jensen RA, Paakinaho V, Fettweis G, Schiltz RL, Wüstner D, Mandrup S, Presman DM, Upadhyaya A, Hager GL. Single-molecule tracking reveals two low-mobility states for chromatin and transcriptional regulators within the nucleus. *bioRxiv*. 2022:2022.2007.2025.501476.
53. Savory JG, Prefontaine GG, Lamprecht C, Liao M, Walther RF, Lefebvre YA, Hache RJ. Glucocorticoid receptor homodimers and glucocorticoid-mineralocorticoid receptor heterodimers form in the cytoplasm through alternative dimerization interfaces. *Mol Cell Biol*. 2001;21(3):781-793.
54. Kiilerich P, Triqueneaux G, Christensen NM, Trayer V, Terrien X, Lombes M, Prunet P. Interaction between the trout mineralocorticoid and glucocorticoid receptors in vitro. *J Mol Endocrinol*. 2015;55(1):55-68.
55. Planey SL, Derfoul A, Steplewski A, Robertson NM, Litwack G. Inhibition of glucocorticoid-induced apoptosis in 697 pre-B lymphocytes by the mineralocorticoid receptor N-terminal domain. *J Biol Chem*. 2002;277(44):42188-42196.
56. Mifsud KR, Reul JM. Acute stress enhances heterodimerization and binding of corticosteroid receptors at glucocorticoid target genes in the hippocampus. *Proc Natl Acad Sci U S A*. 2016;113(40):11336-11341.
57. Le Billan F, Amazit L, Bleakley K, Xue QY, Pussard E, Lhadj C, Kolkhof P, Viengchareun S, Fagart J, Lombes M. Corticosteroid receptors adopt distinct cyclical transcriptional signatures. *FASEB J*. 2018;32(10):5626-5639.
58. Ackermann D, Gresko N, Carrel M, Loffing-Cueni D, Habermehl D, Gomez-Sanchez C, Rossier BC, Loffing J. In vivo nuclear translocation of mineralocorticoid and glucocorticoid receptors in rat kidney: differential effect of corticosteroids along the distal tubule. *Am J Physiol Renal Physiol*. 2010;299(6):F1473-1485.
59. Ronzaud C, Loffing J, Bleich M, Gretz N, Grone HJ, Schutz G, Berger S. Impairment of sodium balance in mice deficient in renal principal cell mineralocorticoid receptor. *J Am Soc Nephrol*. 2007;18(6):1679-1687.
60. Nguyen Dinh Cat A, Ouvrard-Pascaud A, Tronche F, Clemessy M, Gonzalez-Nunez D, Farman N, Jaisser F. Conditional transgenic mice for studying the role of the glucocorticoid receptor in the renal collecting duct. *Endocrinology*. 2009;150(5):2202-2210.
61. Cong L, Ran FA, Cox D, Lin S, Barretto R, Habib N, Hsu PD, Wu X, Jiang W, Marraffini LA, Zhang F. Multiplex genome engineering using CRISPR/Cas systems. *Science*. 2013;339(6121):819-823.
62. Garcia DA, Johnson TA, Presman DM, Fettweis G, Wagh K, Rinaldi L, Stavreva DA, Paakinaho V, Jensen RAM, Mandrup S, Upadhyaya A, Hager GL. An intrinsically disordered region-mediated confinement state contributes to the dynamics and function of transcription factors. *Mol Cell*. 2021;81(7):1484-1498 e1486.
63. Mazza D, Abernathy A, Golob N, Morisaki T, McNally JG. A benchmark for chromatin binding measurements in live cells. *Nucleic Acids Res*. 2012;40(15):e119.

bioRxiv preprint doi: https://doi.org/10.1101/2023.01.26.525745; this version posted January 26, 2023. The copyright holder for this preprint (which was not certified by peer review) is the author/funder, who has granted bioRxiv a license to display the preprint in perpetuity. It is made available under aCC-BY-NC-ND 4.0 International license.

64. Gomez-Sanchez CE, de Rodriguez AF, Romero DG, Estess J, Warden MP, Gomez-Sanchez MT, Gomez-Sanchez EP. Development of a panel of monoclonal antibodies against the mineralocorticoid receptor. *Endocrinology*. 2006;147(3):1343-1348.
65. Heinz S, Benner C, Spann N, Bertolino E, Lin YC, Laslo P, Cheng JX, Murre C, Singh H, Glass CK. Simple combinations of lineage-determining transcription factors prime cis-regulatory elements required for macrophage and B cell identities. *Mol Cell*. 2010;38(4):576-589.

Figure 1

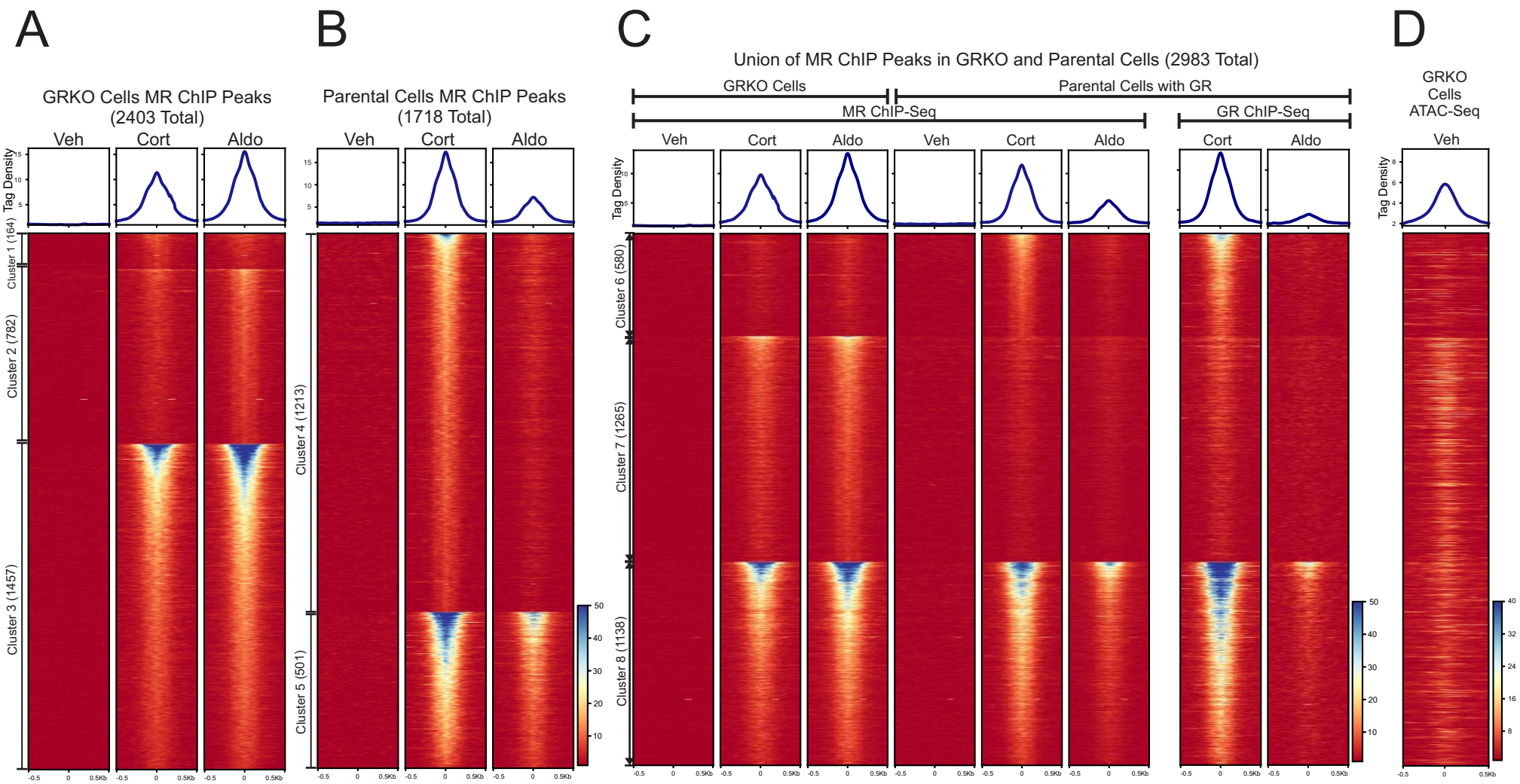
A
GRKO Cells MR ChIP Peaks
(2403 Total)
Veh
Cort
Aldo
Tag Density
Cluster 1 (164)
Cluster 2 (782)
Cluster 3 (1457)
B
Parental Cells MR ChIP Peaks
(1718 Total)
Cluster 4 (1213)
Cluster 5 (501)
C
Union of MR ChIP Peaks in GRKO and Parental Cells (2983 Total)
GRKO Cells
Parental Cells with GR
MR ChIP-Seq
GR ChIP-Seq
Cluster 6 (580)
Cluster 7 (1265)
Cluster 8 (1138)
D
GRKO
Cells
ATAC-Seq
-0.5
0
0.5Kb

Figure 2

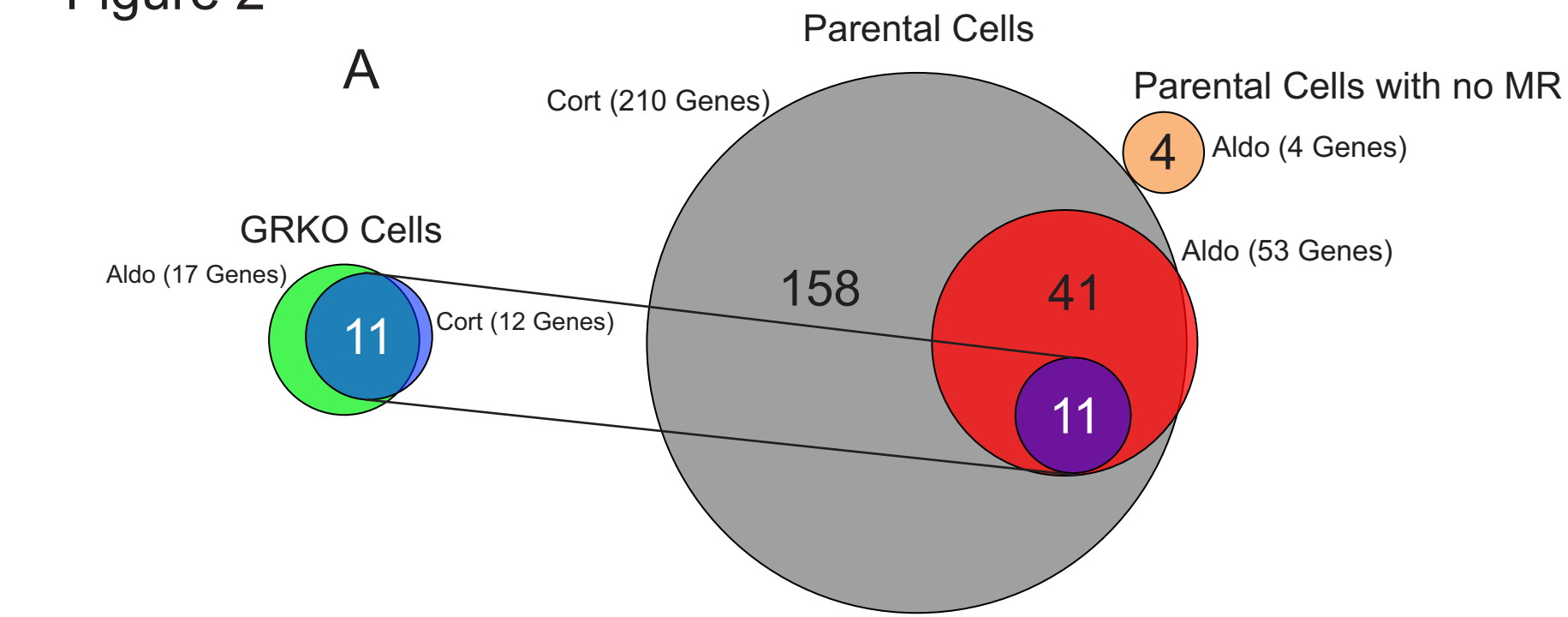
A
Parental Cells
Cort (210 Genes)
Parental Cells with no MR
4
Aldo (4 Genes)
GRKO Cells
Aldo (17 Genes)
11
Cort (12 Genes)
158
41
Aldo (53 Genes)
11

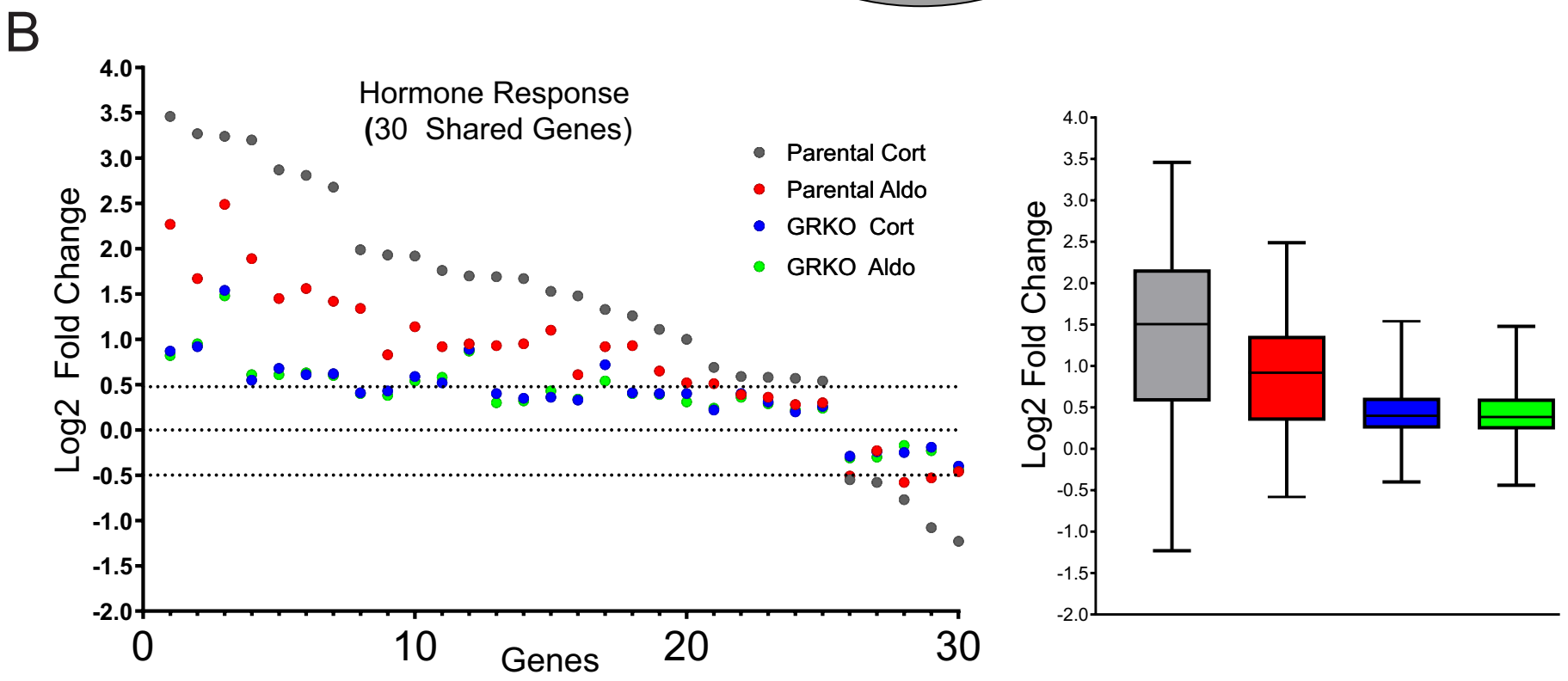
B
Hormone Response
(30 Shared Genes)
Parental Cort
Parental Aldo
GRKO Cort
GRKO Aldo
Log2 Fold Change
Genes
4.0
3.5
3.0
2.5
2.0
1.5
1.0
0.5
0.0
-0.5
-1.0
-1.5
-2.0
0
10
20
30

Figure 3

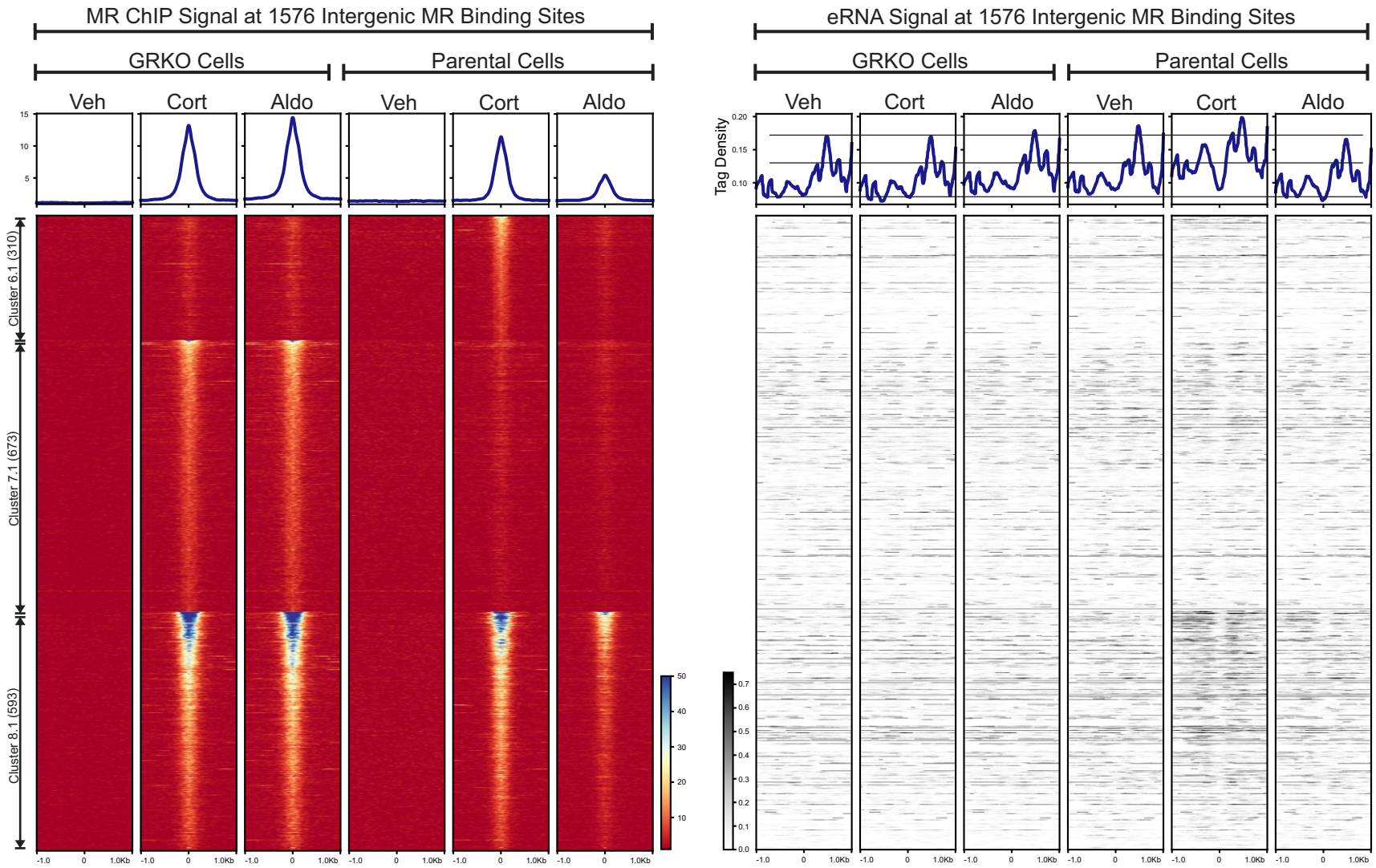
MR ChIP Signal at 1576 Intergenic MR Binding Sites
GRKO Cells
Parental Cells
Veh
Cort
Aldo
Veh
Cort
Aldo
Cluster 6.1 (310)
Cluster 7.1 (673)
Cluster 8.1 (593)
-1.0
0
1.0Kb
eRNA Signal at 1576 Intergenic MR Binding Sites
GRKO Cells
Parental Cells
Tag Density

Figure 4

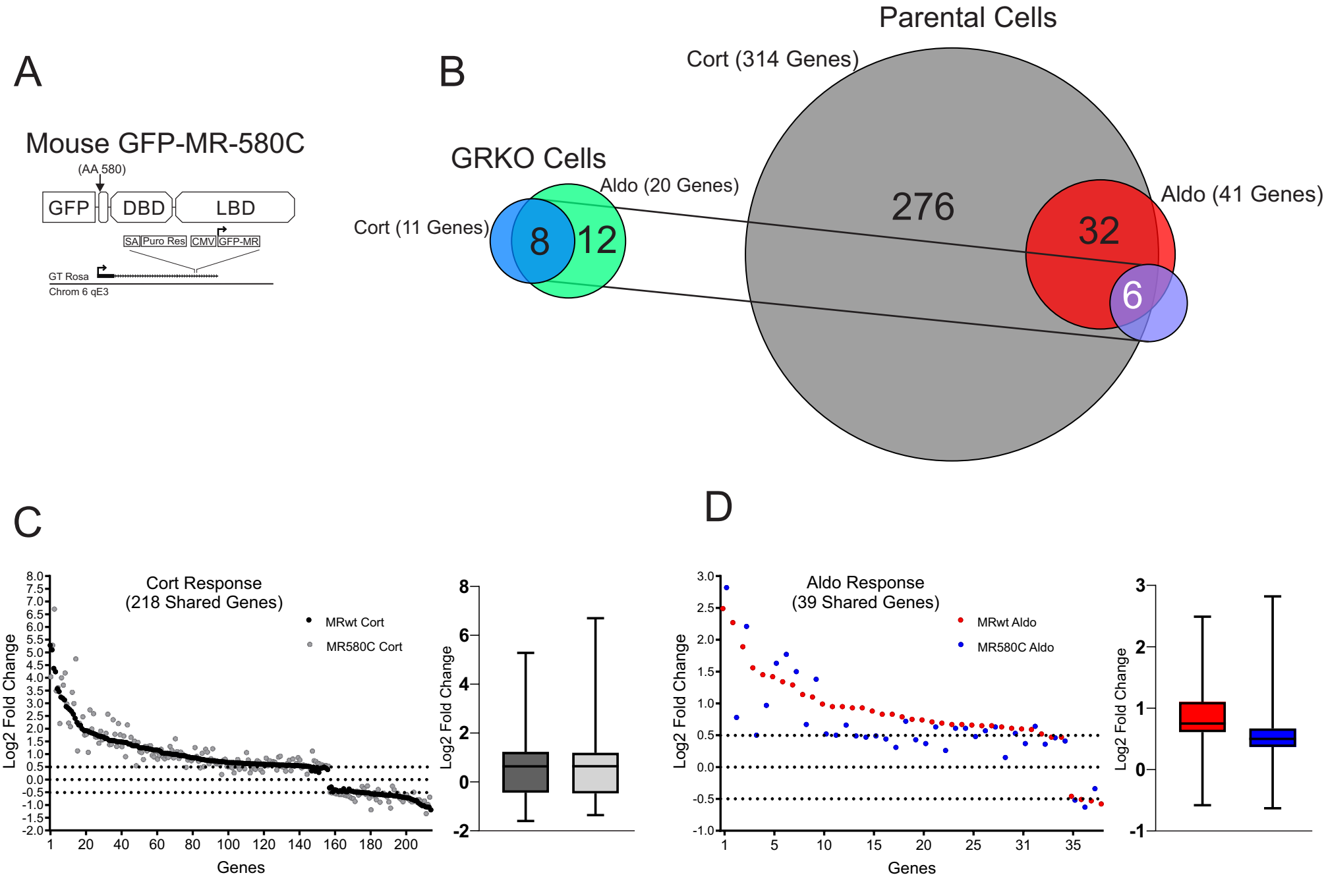
A
Mouse GFP-MR-580C
(AA 580)
GFP
DBD
LBD
SA
Puro Res
CMV
GFP-MR
GT Rosa
Chrom 6 qE3
B
Parental Cells
Cort (314 Genes)
GRKO Cells
Aldo (20 Genes)
Cort (11 Genes)
8
12
276
32
6
Aldo (41 Genes)
C
Cort Response
(218 Shared Genes)
MRwt Cort
MR580C Cort
Log2 Fold Change
Genes
D
Aldo Response
(39 Shared Genes)
MRwt Aldo
MR580C Aldo
Log2 Fold Change
Genes

bioRxiv preprint doi: https://doi.org/10.1101/2023.01.26.525745; this version posted January 26, 2023. The copyright holder for this preprint (which was not certified by peer review) is the author/funder, who has granted bioRxiv a license to display the preprint in perpetuity. It is made available under aCC-BY-NC-ND 4.0 International license.
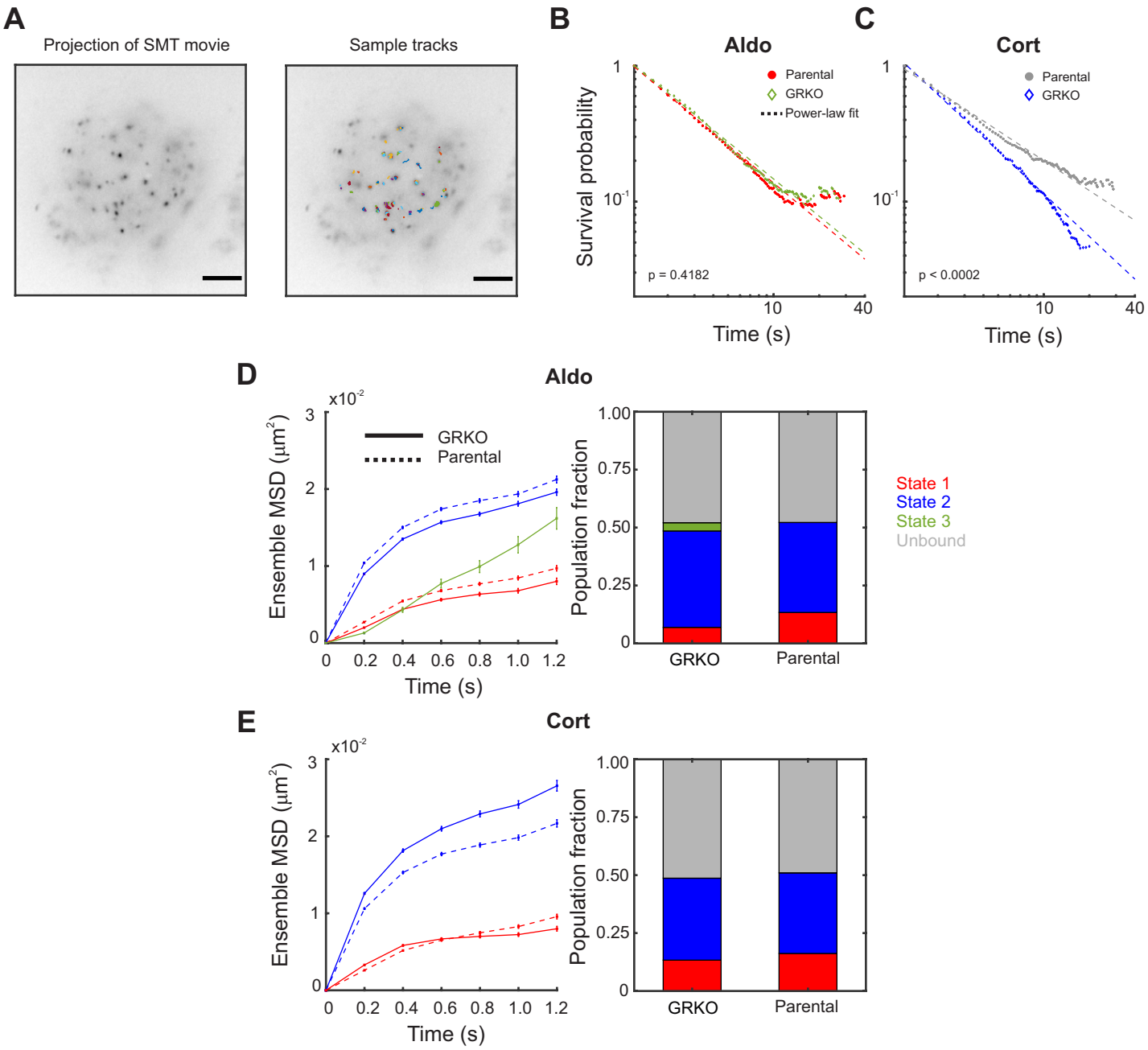
Figure 5